Current Losses at the Front of Silicon Heterojunction Solar Cells

Zachary C. Holman, Antoine Descoeudres, Loris Barraud, Fernando Zicarelli Fernandez, Johannes P. Seif, Stefaan De Wolf, and Christophe Ballif

***Abstract*—The current losses due to parasitic absorption in the indium tin oxide (ITO) and amorphous silicon (a-Si:H) layers at the front of silicon heterojunction solar cells are isolated and quantified. Quantum efficiency spectra of cells in which select layers are omitted reveal that the collection efficiency of carriers generated in the ITO and doped a-Si:H layers is zero, and only 30% of light absorbed in the intrinsic a-Si:H layer contributes to the short-circuit current. Using the optical constants of each layer acquired from ellipsometry as inputs in a model, the quantum efficiency and short-wavelength current loss of a heterojunction cell with arbitrary a-Si:H layer thicknesses and arbitrary ITO doping can be correctly predicted. A 4 cm^2 solar cell in which these parameters have been optimized exhibits a short-circuit current density of 38.1 mA/cm^2 and an efficiency of 20.8%.**

***Index Terms*—Amorphous silicon, heterojunctions, photovoltaic cells, silicon, solar cells.**

I. Introduction

SILICON heterojunction solar cells with open-circuit voltages ($V_{\rm oc}$s) exceeding 700 mV have been reported by several groups [1]–[3], including our own [4], [5]. Such large values are possible because the architecture of heterojunction cells capitalizes on two unique properties of nanometer-thin intrinsic hydrogenated amorphous silicon (a-Si:H) films: their ability to both passivate [6] and drain charge [7] from crystalline silicon surfaces. The former results in several-millisecond effective lifetimes when high-quality wafers are used [5]; the latter permits photogenerated carriers to be extracted without recombination-active contacts that ruin the high lifetimes [8], [9]. Carrier extraction occurs at the front of silicon heterojunction solar cells under the influence of the built-in electric field that is formed when a (typically p-type) doped a-Si:H film is deposited on top of the intrinsic passivation layer, forming the emitter. This emitter is different from the diffused emitters traditionally used in crystalline silicon solar cells in that low-resistance lateral conduction through it across millimeter length scales is not possible, requiring a transparent conductive oxide (TCO) layer to transport charge laterally to the metallic front electrode grid.

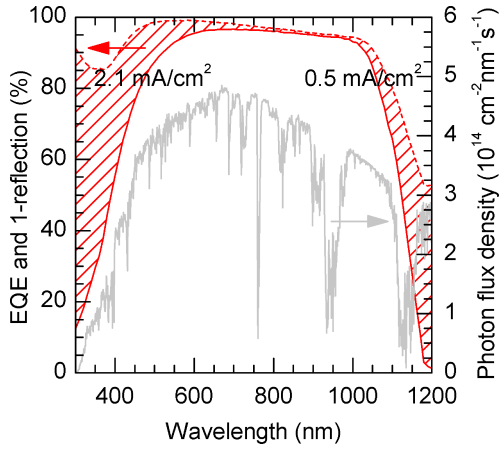

Fig. 1. EQE (red, solid) and 1-reflection (red, dashed) of a high-$J_{\rm sc}$ silicon heterojunction solar cell. The shaded area indicates parasitic absorption, and the associated current losses below 600 nm and above 1000 nm are given, assuming an AM 1.5G spectrum (gray).

Regrettably, the a-Si:H and TCO films at the front of silicon heterojunction solar cells absorb light parasitically, so that the gains they enable in $V_{\rm oc}$ are partially offset by losses in short-circuit current density ($J_{\rm sc}$). The external quantum efficiency (EQE) and absorption (1-reflection) of a 250-μm-thick heterojunction solar cell with $J_{\rm sc} = 38.1$ mA/cm^2 are shown in Fig. 1. The EQE can be written as the sum of the contributions from each layer in a solar cell

$$\mathrm{EQE}(\lambda) = \sum_m A_m(\lambda)\ \beta_m \tag{1}$$

where $A_m(\lambda)$ is the fraction of incident light of wavelength λ absorbed in the mth layer, and β_m is the probability that light absorbed in this layer will result in charge carrier collection. (β_m can be thought of as a per-layer internal quantum efficiency; we neglect any wavelength dependence.) The shaded area between the EQE and 1-reflection curves in Fig. 1 represents losses from light that is absorbed but does not produce collected carriers, i.e., from nonunity β. We use the term "parasitic absorption" here to refer to such losses, which include both absorption that does not create an electron-hole pair (e.g., free-carrier absorption) and recombination before collection. When integrated over the AM 1.5G spectrum (shown in gray), parasitic absorption

Manuscript received September 9, 2011; revised October 27, 2011; accepted November 1, 2011. Date of publication January 12, 2012; date of current version January 30, 2012. This work was supported by the European Union Seventh Framework Programme (FP7/2007-2013), Collaborative Project "20plμs" with the full title: "Further development of very thin wafer based c-Si photovoltaics" under Grant 256695, by Axpo Naturstrom Fonds, Switzerland, and by the Swiss Commission for Technology and Innovation under Project 9908 PFNMM-NM.

The authors are with the Photovoltaics and Thin-Film Electronics Laboratory, Institute of Microengineering, Ecole Polytechnique Fédérale de Lausanne, Neuchâtel 2000, Switzerland (e-mail: zachary.holman@epfl.ch; antoine.descoeudres@epfl.ch; loris.barraud@epfl.ch; fernando.zicarelli@epfl.ch; johannes.seif@epfl.ch; stefaan.dewolf@epfl.ch; christophe.ballif@epfl.ch).

Color versions of one or more of the figures in this paper are available online at http://ieeexplore.ieee.org.

Digital Object Identifier 10.1109/JPHOTOV.2011.2174967

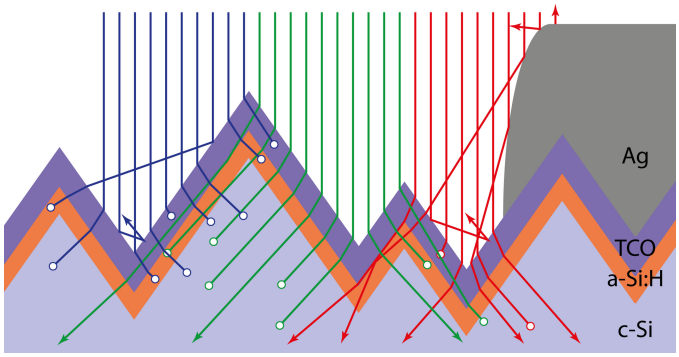

Fig. 2. Schematic of representative paths taken by UV (blue), visible (green), and IR (red) photons at the front of a silicon heterojunction solar cell. Absorption is marked by open circles; arrows indicate photons that continue beyond the schematic. The thicknesses of the ITO and a-Si:H layers are exaggerated in relation to the pyramid dimensions, but all angles are represented accurately for reasonable assumed refractive indices.

amounts to 2.1 mA/cm^2 of current lost at wavelengths below 600 nm and 0.5 mA/cm^2 lost above 1000 nm. All of the short-wavelength losses and some of the IR losses occur at the front of the cell. Consequently, a relative efficiency increase of over 5% is possible—even in this optimized cell—by mitigating parasitic absorption in the front TCO/a-Si:H stack.

Fig. 2 illustrates representative interactions between light of three wavelengths and the front of a heterojunction solar cell. A few percent of photons are reflected by the front metallization grid and at the air/TCO interface. The associated current loss is minimized by restricting the TCO thickness to approximately 75 nm so that the layer serves as an antireflection coating with a reflection minimum near 600 nm. TCOs, of which indium tin oxide (ITO) is the most common, absorb both in the UV above their bandgaps and in the IR due to excitation of free carriers. UV and visible light is absorbed in the a-Si:H layers, which have an optical bandgap of approximately 1.7 eV. Others have demonstrated that absorption in the heavily doped a-Si:H p-layer is parasitic due to its high defect density, and that $J_{\rm sc}$ also decreases with i-layer thickness [3], [10]–[13]. Light with wavelengths less than 1000 nm that passes through the front layer stack is absorbed in the crystalline silicon wafer. Due to the millisecond minority carrier effective lifetimes in heterojunction solar cells, electron-hole pairs generated in the wafer are collected with roughly 100% efficiency ($\beta_{\rm Si} = 1$). Longer wavelengths are weakly absorbed in the wafer and may be absorbed in both the front and rear TCOs as the light traverses the cell multiple times (not shown).

In this paper, we seek a complete accounting of all parasitic absorption in the front ITO, a-Si:H i-, and a-Si:H p-layers of n-type silicon heterojunction solar cells, focusing on the blue response of the cells. IR losses in the ITO layers will be treated in detail in another paper. We measure the quantum efficiency and current-voltage characteristics of heterojunction cells with varying ITO carrier density, p-layer thickness, and i-layer thickness. In each case, we omit select layers, allowing us to isolate—and ultimately predict, with the help of an optical model—the current losses in each layer.

II. Experimental

Silicon heterojunction solar cells were fabricated on n-type float-zone wafers [(100), 4 Ω·cm, 280 μm] after alkaline texturing and cleaning. Intrinsic and n-type a-Si:H layers were deposited via plasma-enhanced chemical vapor deposition (PECVD) on the rear side of all wafers using a modified industrial KAI-M reactor operated at very high frequency [4]. a-Si:H i- and p-layers were deposited on the front side of some wafers either in the KAI reactor (when co-deposition was required on several samples) or in a laboratory-scale INDEOtec PECVD reactor operated at radio frequency (when deposition on individual samples with varying layer thicknesses was required) [5]. Both reactors have produced 4 cm^2 heterojunction solar cells with efficiencies greater than 20.5% and $V_{\rm oc}$s over 720 mV [5]. Prior to deposition, wafers were dipped in diluted hydrofluoric acid to remove native oxide, and samples were either stored air-free or re-dipped if transfer between the two reactors was required. ITO was sputtered from a In_2O_3:Sn target onto both sides of the wafers; the doping density was varied by adjusting the flow of oxygen gas into the chamber [14]. A silver reflector was sputtered onto the rear side of all wafers, and a silver electrode grid was screen-printed onto the front of some samples to complete the solar cells. A low-temperature annealing step is required to cure the silver paste, and samples that were not screen-printed (hereafter called test structures) underwent this step in order to simulate finished devices. The test structures were used for quantum efficiency measurements (no front metallization), while current-voltage measurements were performed on the completed cells. Data from current-voltage measurements presented in this paper each represent the mean value of three cells on one wafer, and error bars correspond to the standard deviation of the mean. Note that these error bars do not take into account variability in, e.g., wafer cleaning and plasma reactor conditioning over time.

Glass substrates witnessed all depositions and were used to characterize the layers after annealing. a-Si:H film thicknesses and complex refractive indices were extracted from spectroscopic ellipsometry measurements using a Tauc-Lorentz model. Determining the optical constants of ITO films was more difficult, but satisfactory results were obtained by simultaneously fitting transmission spectra and multi-angle ellipsometric data with a combined Drude-Tauc-Lorentz model that included a surface roughness layer [15]. ITO film thickness was verified with profilometry, and electron mobility and density were determined from Hall measurements. The film thicknesses reported throughout this paper are those on the pyramidally textured silicon surfaces, calculated by dividing the measured values on flat glass by a theoretical geometric factor of 1.73. We have confirmed this factor by comparing the thicknesses of films co-deposited on flat glass and textured wafers (determined by reflection minima).

Optical models to understand and compliment experimental results were constructed using the freeware program OPAL [16],

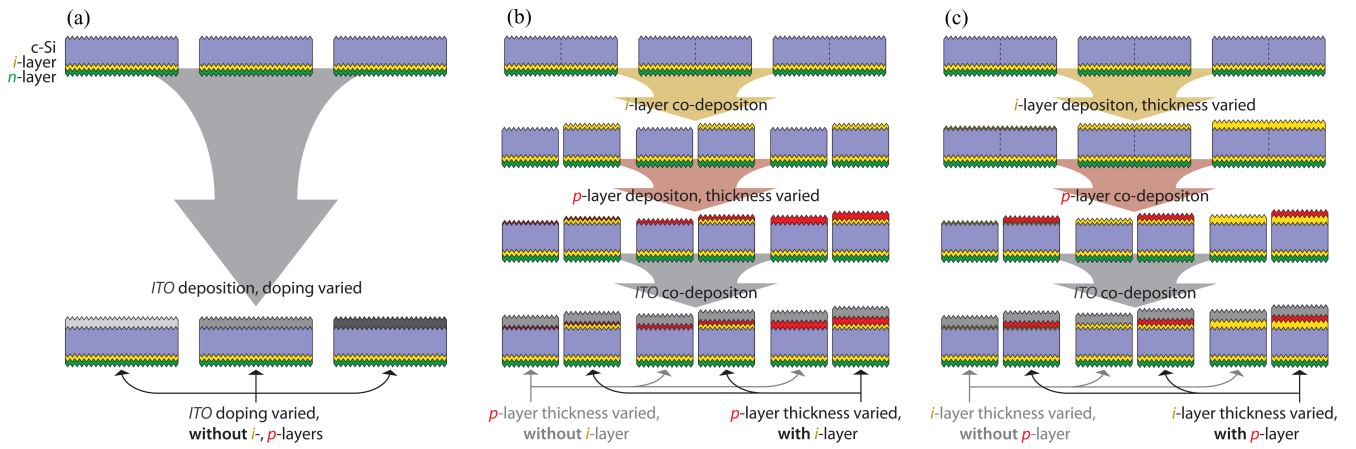

Fig. 3. Schematic diagram of the fabrication of test structures used in the (a) ITO doping, (b) p-layer thickness, and (c) i-layer thickness experiments. ITO and silver films were subsequently sputtered onto the rear sides of all samples.

[17]. For each deposited film, a new material was defined in the program using the complex refractive index of that film determined from ellipsometry. Layers were then assembled to mirror the measured structures using experimentally determined thicknesses, and the absorption in the wafer $A_{\mathrm{Si}}(\lambda)$ was calculated. The program uses a generalized path analysis in which the fraction of light following a given path is taken from ray tracing, and can handle textures like random pyramids in addition to flat geometries. $A_{\mathrm{Si}}(\lambda)\ \beta_{\mathrm{Si}} = A_{\mathrm{Si}}(\lambda)$ was then compared to measured EQE spectra to evaluate if the collected current comes exclusively from light absorbed in the wafer. Similarly, $A_{\mathrm{Si}}(\lambda)/\sum A_m(\lambda)$ was compared to internal quantum efficiency (IQE) spectra.

Three experiments make up the bulk of this paper. Together they deconstruct and rebuild the front of heterojunction solar cells, introducing a perturbation into one layer at a time in order to determine the layer's influence on quantum efficiency. In one experiment, shown schematically in Fig. 3(a), current losses in front ITO films of varying doping density were examined by measuring the quantum efficiency of test structures for which the front i- and p-layers were omitted. Without junctions to drive these devices, an applied reverse bias of 1 V was required during measurement to extract carriers and produce the near 100% IQEs observed between 700 and 1000 nm in completed cells that include i- and p-layers. The refractive indices n and extinction coefficients k of the ITO films—which were used in OPAL—are shown in Fig. 4(a).

In a second experiment, illustrated in Fig. 3(b), current losses in the p-layer were assessed by varying the layer thickness and observing the change in quantum efficiency. The front i-layer was omitted in half of the test structures; half received a co-deposited i-layer prior to p-layer deposition. ITO was co-deposited on all samples. Fig. 4(b) displays n and k for all the p-layers and the sole i-layer. The optical constants of the p-layers are similar though not identical, and their variation is not correlated with layer thickness. Consequently, average values of n and k were used in OPAL so that a single p-type a-Si:H material could be defined and its thickness varied to simulate our experiments.

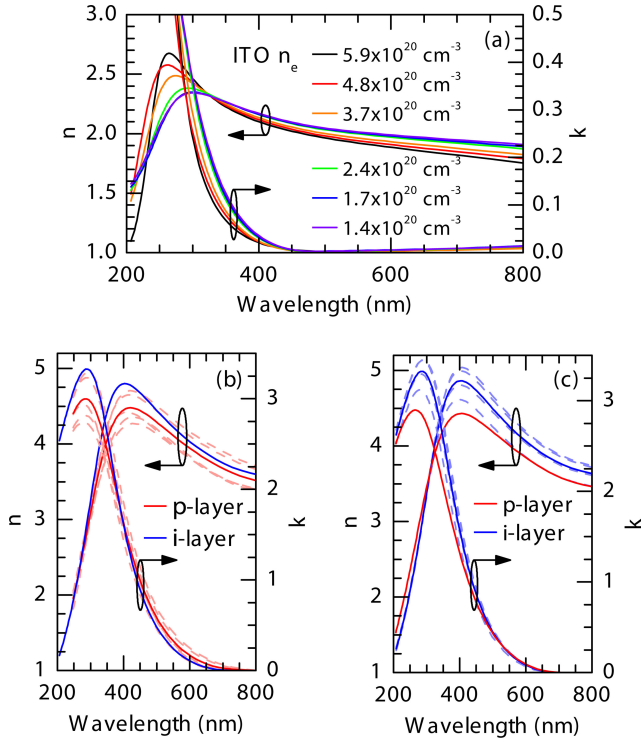

Fig. 4. Refractive indices and extinction coefficients extracted from ellipsometry of the (a) ITO layers used in the ITO doping study, and the a-Si:H layers used in the (b) p-layer thickness study and (c) i-layer thickness study. In (b), p-layers of varying thickness are represented by dashed lines, whereas their average and the sole i-layer are depicted as solid lines. Similarly, i-layers of varying thickness are represented by dashed lines in (c), whereas their average and the sole p-layer are depicted as solid lines.

In a third, complementary experiment, front i-layer thickness was varied in test structures, half of which then received co-deposited p-layers [see Fig. 3(c)]. ITO was again co-deposited on all samples. n and k increase monotonically with i-layer

thickness, reflecting intentional heterogeneity in this layer (see [5]). Nonetheless, the average optical constants of the i-layers were used in OPAL, for simplicity [see Fig. 4(c)].

III. Results and Discussion

A. Losses in the Front ITO

The front TCO layer in heterojunction solar cells acts simultaneously as a lateral transport medium, a window layer, and an anti-reflection coating. Consequently, the ideal layer is composed of a material with metallic conductivity, no absorption, and a refractive index that is the geometric mean of those of silicon and air. While no such material is known, tuning the electron density n_e of existing TCOs via doping allows one to trade, e.g., absorption losses for resistance losses.

The quantum efficiencies of test structures in which the front ITO doping was varied are shown in Fig. 5(b), and the absorption spectra of ITO films on glass witness substrates appear in Fig. 5(a). The test structures have no i- or p-layers so that any short-wavelength losses are expected to be attributable to absorption in the ITO. In Fig. 5(a), bandgap absorption is observed below 450 nm and is pushed to lower wavelengths for higher n_e due to filling of states in the bottom of the conduction band (Burstein-Moss effect) [15], [18]–[20]. This absorption translates into a loss in IQE, seen as a separation of the EQE and 1-reflection curves in Fig. 5(b), and the Burstein-Moss effect results in improved UV quantum efficiency for more conductive ITOs. Unfortunately, the IR quantum efficiency (not shown) exhibits the reverse trend since free-carrier absorption increases with n_e [see Fig. 5(a)]. Additionally, UV reflection from the test structure surface increases with higher ITO doping because of poorer index matching [see Fig. 4(a)].

In Fig. 5(a) and (b), the results of OPAL models for the appropriate sample geometries are shown as solid lines. In Fig. 5(b), the curves plotted are the percentage of light absorbed in the silicon wafer, $A_{\mathrm{Si}}(\lambda)$. With no i- or p-layers, (1) gives $\mathrm{EQE}(\lambda) = A_{\mathrm{Si}}(\lambda)$ if $\beta_{\mathrm{ITO}} = 0$, which is to be expected. The OPAL spectra fit the measured EQE data well, validating this interpretation and confirming that ITO absorption accounts for all short-wavelength current losses in these test structures. In both Fig. 5(a) and (b), the model tracks the data as the bandgap shifts, although the simplistic Drude-Tauc-Lorentz model used to fit the ITO ellipsometry and transmission data results in an underestimate of absorption at wavelengths greater than 450 nm. Fig. 5(c) summarizes the influence of the front ITO doping on quantum efficiency by plotting measured IQEs and modeled $A_{\mathrm{Si}}(\lambda)/\sum A_m(\lambda)$ spectra at four wavelengths as a function of n_e.

Current-voltage measurements of complete (i- and p-layers included) solar cells with varying front ITO doping reveal that the Burstein-Moss effect does little to offset free-carrier absorption losses, leading to a linear decrease in J_{sc} with increasing n_e (see Fig. 6). Hence, from an optical perspective, the best ITO has the lowest n_e. However, electrical losses in the ITO trend in the opposite direction. Fill factor (FF) increases with increasing n_e and saturates for $n_e > 5 \times 10^{20}$ cm^{-3} (for the finger spacing used here), for which the ITO sheet resistance no longer contributes significantly to series resistance. Note that the thickness and mobility of the ITO films in Fig. 6 differ by less than 5%. n_e is thus inversely proportional to sheet resistance, and the abscissae could equivalently be labeled as ranging from 287 to 57 Ω/sq. The overall efficiency of the cells peaks when the balance between J_{sc} and FF losses is optimized, which occurs for $n_e \approx 3 \times 10^{20}$ cm^{-3} (100 Ω/sq). ITO layers of approximately this doping are used throughout the rest of this paper.

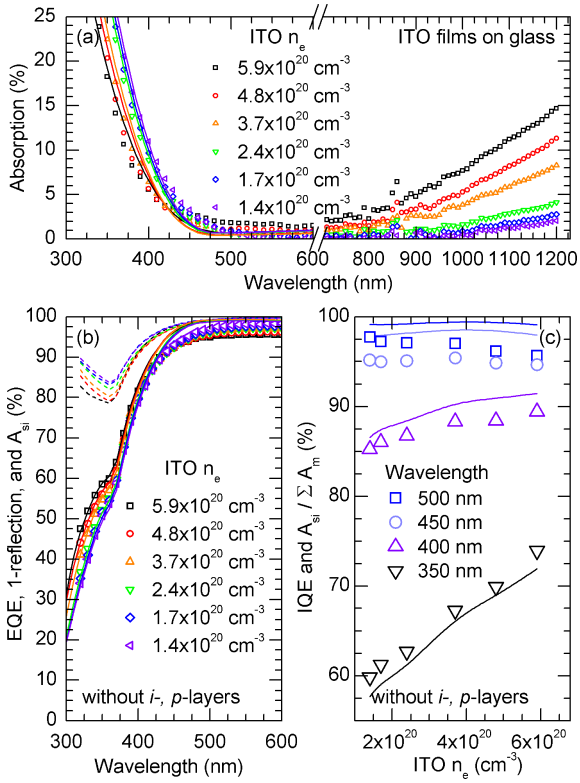

Fig. 5. (a) Measured (symbols) and modeled (solid lines) absorption spectra of ITO films of varying doping on glass. (b) EQE (symbols), 1-reflection (dashed lines), and calculated absorption in the wafer (solid lines) of test structures without i- or p-layers and with ITO layers co-deposited with those in (a). EQE measurements were performed under a 1 V reverse bias. (c) Measured IQE (symbols) and fraction of absorbed light absorbed in the wafer (solid lines) at four wavelengths as a function of front ITO electron density.

B. Losses in the p-Layer

Tanaka *et al*. first demonstrated that the defective p-layer in n-type silicon heterojunctions reduces short-wavelength quantum efficiency and thus cell J_{sc} [11], and the analysis was extended on untextured solar cells by Fujiwara and Kondo [10]. Jensen *et al*. found that carriers generated in thick n-type a-Si:H emitters of heterojunctions on p-type wafers without i-layers have an 85% chance of recombining at short circuit [21]. Parsing the parasitic absorption losses in the i- and p-layers (the i-layer has also been shown to decrease J_{sc}) is challenging in cells that include both layers, and has not yet been performed. Fig. 7(a) plots the blue quantum efficiency of test structures with no i-layer, and p-layers ranging in thickness from 0 to 23 nm. With $\beta_{\mathrm{ITO}} = 0$ determined from the previous experiment, (1) reduces to $\mathrm{EQE}(\lambda) = A_p(\lambda)\ \beta_p + A_{\mathrm{Si}}(\lambda)$, and the efficiency

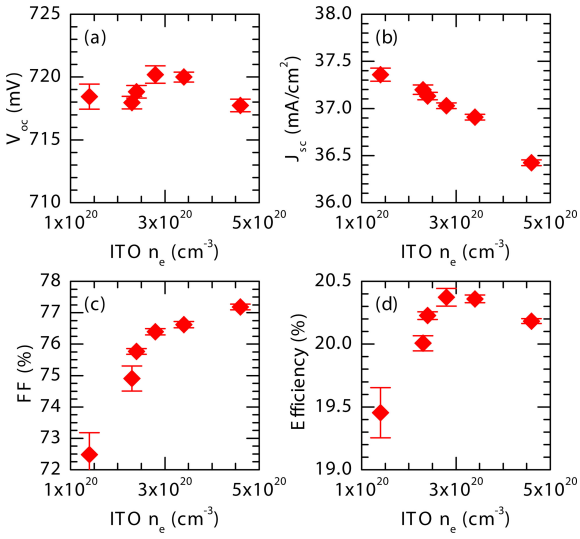

Fig. 6. Output characteristics of 4 cm^2 solar cells with varying front ITO doping. Each data point represents the average value of three cells.

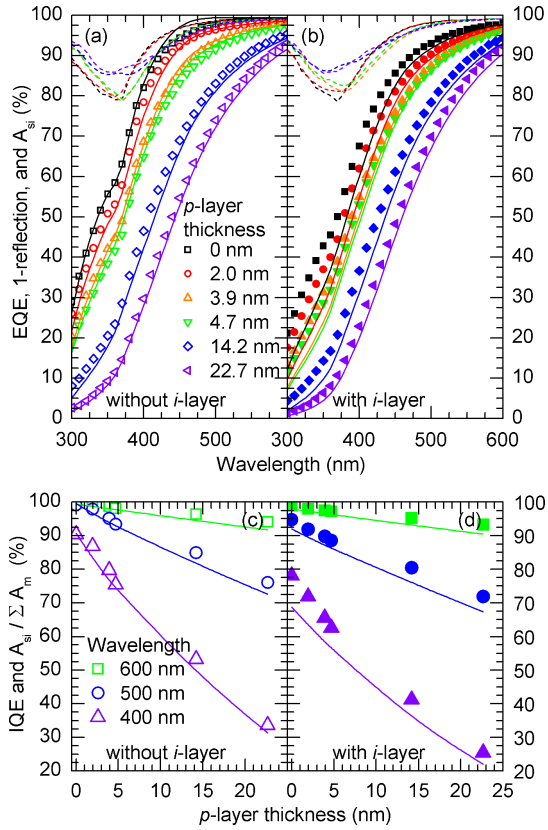

Fig. 7. EQE (symbols), 1-reflection (dashed lines), and calculated absorption in the wafer (solid lines) of test structures with p-layers of varying thickness (a) without and (b) with i-layers. For the test structures without i-layers, surface recombination was greatly enhanced and a small (0.2 to 0.4 V) reverse bias was needed to reach near-100% IQEs. A 1 V reverse bias was used for the sample with no p- or i-layers. Measured IQE (symbols) and fraction of absorbed light absorbed in the wafer (solid lines) at three wavelengths as a function of p-layer thickness for test structures (c) without and (d) with i-layers.

with which carriers photogenerated in the p-layer are collected can be determined. The solid curves again show $A_{\mathrm{Si}}(\lambda)$ for each test structure, as calculated with OPAL. These curves could be mistaken for fits to the experimental data but in fact they correspond to predicted EQEs only if $\beta_p = 0$. The associated $A_{\mathrm{Si}}(\lambda)/\sum A_m(\lambda)$ spectra calculated with OPAL at three wavelengths appear in Fig. 7(c) and fit the measured IQE data well; apparently all absorption in the p-layer is parasitic.

The p-layer is deposited at higher hydrogen dilution than the i-layer, which may lead to undesired epitaxial growth at the wafer surface [22]. The new p-layer/wafer interface created in the test structures—be it epitaxial or not—differs from that in our standard solar cells, and it is possible that the above quantum efficiency analysis cannot be extended to devices with i-layers. Fig. 7(b) and (d) display the results of the same p-layer thickness experiment, but with a co-deposited, 6.4-nm-thick i-layer inserted before p-layer deposition. The EQEs of these test structures closely resemble those of their i-layer-free counterparts, but they are lower due to absorption in the i-layer. This is consistent with the additive nature of (1) and suggests that—from a quantum efficiency perspective—the devices are not fundamentally changed by removing, e.g., the i-layer. Thus, at least for some layers, β may be independent of the presence or absence of other layers. Note that $A_{\mathrm{Si}}(\lambda)/\sum A_m(\lambda)$, as calculated with OPAL underestimates the IQE when the i-layer is included regardless of p-layer thickness, indicating that the collection efficiency of carriers generated in this layer is *not* zero.

The output characteristics of solar cells (i-layer included) with varying p-layer thickness are given in Fig. 8. Consistent with reports by Tanaka *et al.* and Fujiwara and Kondo [10], [11], V_{oc} is unchanged for p-layers as thin as 3 nm and J_{sc} falls linearly with increasing thickness due to the parasitic visible and UV absorption. Given that transmission through the p-layer decreases exponentially with its thickness, it is not immediately obvious why J_{sc} would exhibit a linear dependence; this will be discussed shortly. Unlike Tanaka *et al.* and Fujiwara and Kondo, we observe an increase in FF across all p-layer thicknesses investigated, the source of which is still unclear. Cell efficiency is dominated by the J_{sc} trend so that an increase of 0.04% absolute is achieved for each nanometer reduction of the p-layer thickness, at least down to 3 nm.

C. Losses in the i-Layer

The quantum efficiencies of test structures with no p-layers and i-layers 0 to 13 nm thick appear in Fig. 9(a). The magnitude of the current loss due to absorption in the i-layer is striking, and appears to be at odds with results from a-Si:H p-i-n solar cells in which the i-layer is the principal absorbing medium. The curves are insensitive to applied reverse bias during measurement, indicating that the loss does not stem from the missing field a p-layer would provide. The percentage of light absorbed in the wafer calculated with OPAL leads to a significant underestimate of the EQE and IQE at wavelengths below 450 nm [see Fig. 9(c)]; that this underestimate is not continued at higher wavelengths is due to the poor estimation of A_{ITO} at these wavelengths [see Fig. 5(c) and the EQE curve in Fig. 9(a) for the test structure with no i-layer].

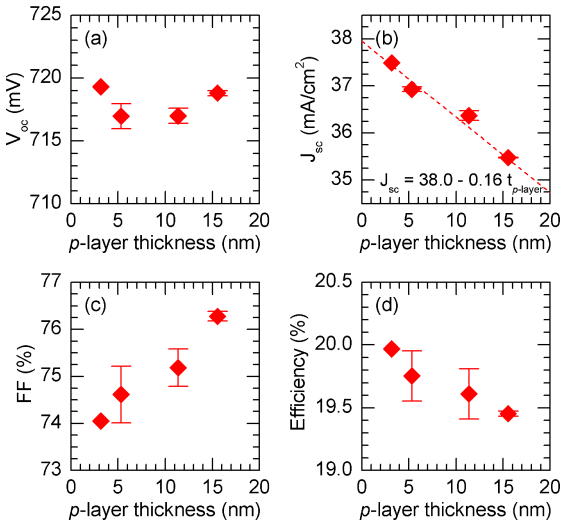

Fig. 8. Output characteristics of 4 cm^2 solar cells with varying p-layer thickness. Each data point represents the average value of three cells, save the data for the thinnest layer, for which only one cell was measured. The dashed line in (b) is the calculated dependence of J_{sc} on p-layer thickness.

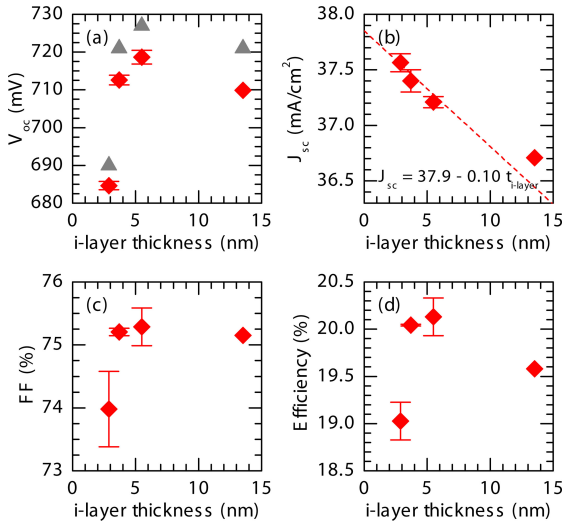

Fig. 10. Output characteristics of 4 cm^2 solar cells with varying i-layer thickness. Each data point represents the average value of three cells, save the data for the thickest layer, for which only one cell was measured. The gray triangles in (a) represent the implied V_{oc}s of the cells prior to ITO deposition and metallization, determined from quasi-steady-state photoconductance (Sinton) measurements. The dashed line in (b) is the calculated dependence of J_{sc} on i-layer thickness.

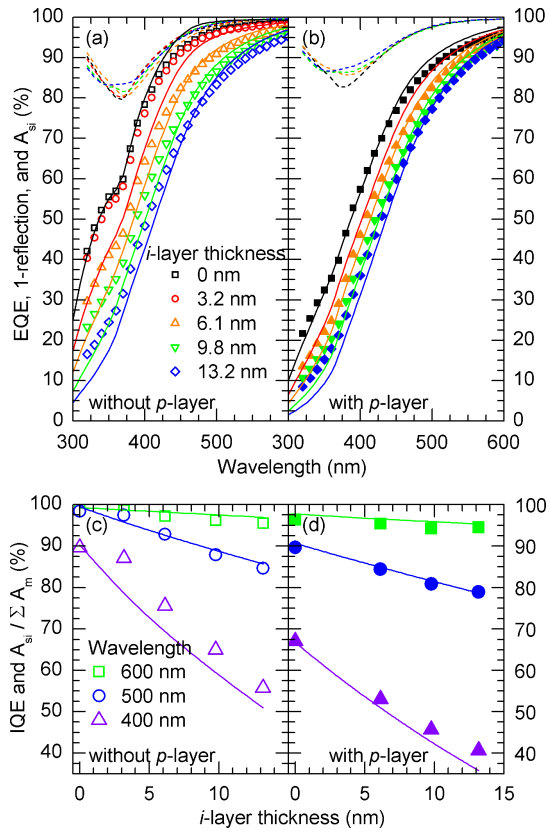

Fig. 9. EQE (symbols), 1-reflection (dashed lines), and calculated absorption in the wafer (solid lines) of test structures with i-layers of varying thickness (a) without and (b) with p-layers. For the test structure in (b) without an i-layer, a 0.2 V reverse bias was needed to reach near-100% IQE. A 1 V reverse bias was used for the sample with no p- or i-layers. Measured IQE (symbols) and fraction of absorbed light absorbed in the wafer (solid lines) at three wavelengths as a function of i-layer thickness for test structures (c) without and (d) with p-layers.

The i-layer thickness experiment is duplicated in Fig. 9(b) and (d), but with the addition of a co-deposited, 7.9-nm-thick p-layer. The quantum efficiency curves are again like those of the test structures in which one a-Si:H layer was omitted, reaffirming the utility of studying samples with missing layers in order to isolate sources of current loss. As in Fig. 7(d), OPAL reveals that the current collected is slightly higher than what could be produced by the light absorbed in the wafer alone. For all three sets of test structures employing i-layers, we have now observed that not all absorption in the i-layer is parasitic. From (1), EQE(λ) = $A_i(\lambda)$ β_i + $A_{\mathrm{Si}}(\lambda)$ regardless of whether a p-layer is present, as β_p = β_{ITO} = 0. β_i can be estimated by calculating $A_i(\lambda)$ and $A_{\mathrm{Si}}(\lambda)$ for a given sample with OPAL, and adjusting β_i to match the experimental EQE curve. For all solar cells with i-layers, fits yield $0.2 < \beta_i < 0.5$, and thus we estimate $\beta_i = 0.3 \pm 0.2$. The large uncertainty reflects potential dependences of the collection efficiency on wavelength and i-layer thickness, which were not studied in detail. Note that, if minority carriers generated in the i-layer recombine at the i/p interface (or the i/ITO interface for samples without p-layers) rather than in the bulk of the i-layer, β_i is expected to have a thickness dependence—particularly at long, uniformly absorbed wavelengths—as diffusion against the built-in field in the i-layer to the interface becomes improbable. No such thickness dependence is observed for the data in Fig. 9, but the range of i-layers investigated here may be too small.

Short-wavelength parasitic absorption in the i-layer causes a steady decrease in J_{sc} in completed cells (p-layer included; see Fig. 10). A minimum tolerable thickness is set, however, by the V_{oc}, which drops rapidly for i-layers thinner than 4 nm, triggering a small drop in FF as well. Others have observed this trend previously [10]–[12]. Consistent with the defect pool model [23], De Wolf and Kondo found that the defect formation

energy in an a-Si:H i-layer is lowered when a p-layer is deposited on it, since the Fermi energy E_F in the i-layer is pulled away from mid gap [24]. Schulze *et al*. have extended this argument and posited that E_F—and thus the defect density—at the heterointerface will vary with i-layer thickness, and $V_{\rm oc}$ should thus decrease for thinner i-layers [25]. This does not explain our results, however, as an AFORS-HET model reveals that the decrease in E_F at the heterointerface is small and gradual as the i-layer thickness increases from 3 to 15 nm [26]. Furthermore, we often observe an increase—not a decrease—in minority carrier effective lifetime after p-layer deposition (6 nm thick i-layer), indicating that the benefit of field-effect passivation outweighs the drawback of E_F-shift-induced defect generation for our layers. An alternative explanation originally proposed by De Wolf and Beaucarne is that minority carriers in the wafer probe bulk defects in the a-Si:H layers up to their tunneling depth [27], which Schulze *et al*. have calculated to be approximately 2.7 nm [25]. One anticipates that the minority carrier lifetime—and thus $V_{\rm oc}$—will fall rapidly if the defective p-layer is within this tunneling depth, as is observed in Fig. 10(a). Overall cell efficiency is maximized for layers that are thick enough to passivate, but no thicker. Fujiwara and Kondo found an optimum i-layer thickness of 4 nm on polished wafers [10]; we find that this same value applies to textured wafers for the layers used here.

D. Predicting Losses

Having identified and modeled all current losses at the front of silicon heterojunction solar cells, we can fabricate arbitrary structures in OPAL and predict the resulting $J_{\rm sc}$ loss by integrating the calculated EQE over the solar spectrum. Fig. 11 compares the cumulative current lost at wavelengths below 600 nm in heterojunctions with the same ITO ($n_e = 3.7 \times 10^{20}$ cm^{-3}) and a-Si:H layers up to 12 nm thick. A cell with no parasitic absorption (no a-Si:H layers, silicon nitride in place of the front ITO) was used as a reference ($J_{\rm sc}$ loss = 0). For all cells, $\beta_i = 0.3$ was used to account for the non-zero collection efficiency in this layer.

Comparing the cell without i- and p-layers in Fig. 11 to all others, it is apparent that the short-wavelength loss in the front ITO is minor. Front ITO layers should thus always be selected for their IR transparency and sheet resistance, and without regard for their bandgap absorption. Fig. 11 also reveals that if the thickness of one a-Si:H layer is fixed, varying the other results in a nearly linear change in current loss, as was observed experimentally in Figs. 8(b) and 10(b). This occurs because the majority of solar photons have wavelengths greater than 450 nm (see Fig. 1). For these wavelengths, the absorption coefficient of a-Si:H is sufficiently small that the exponential decrease in transmitted light intensity is approximately linear over the range of thicknesses investigated [see Figs. 7(d) and 9(d)]. The dashed lines in Figs. 8(b) and 10(b) are calculated from OPAL and they fit the data well. The slopes differ because the collection efficiencies and absorption coefficients of the i- and p-layers differ.

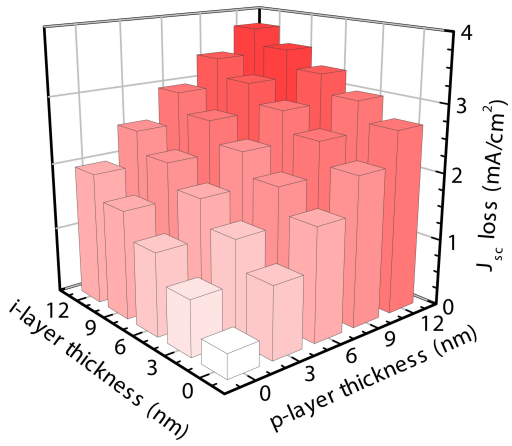

Fig. 11. Calculated loss in $J_{\rm sc}$ of heterojunction cells with varying i- and p-layer thicknesses due to parasitic absorption below 600 nm. Values are relative to a cell with no a-Si:H layers and with a transparent silicon nitride anti-reflection coating in place of the front ITO. The optical constants used were those of the ITO with $n_e = 3.7 \times 10^{20}$ cm^{-3} in Fig. 4(a), and the i- and p-layers in Fig. 4(b).

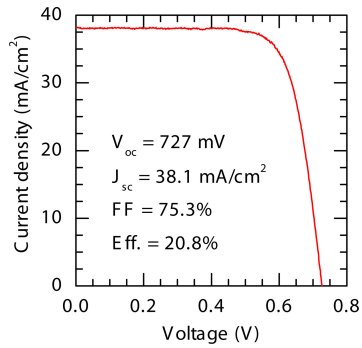

Fig. 12. Current-voltage characteristic of a silicon heterojunction solar cell with an optimized front ITO film and a thin p-layer in order to increase $J_{\rm sc}$.

E. Cell Results

Fig. 12 shows the current-voltage characteristic of a high-$J_{\rm sc}$ silicon heterojunction solar cell in which several of the concepts explored in this paper were integrated, including an optimized front ITO film and a thin p-layer. A respectable FF of over 75% is maintained despite a $J_{\rm sc}$ in excess of 38 mA/cm^2. Aided by an excellent $V_{\rm oc}$ of 727 mV, this results in an efficiency of 20.8% for this 4 cm^2 device. The quantum efficiency of this cell is shown in Fig. 1.

IV. Conclusion

We have isolated and quantified the $J_{\rm sc}$ losses in the ITO/a-Si:H layer stack at the front of silicon heterojunction solar cells. They may be reduced by decreasing ITO doping and a-Si:H layer thickness, improving cell efficiency until $V_{\rm oc}$ and FF degrade. Further improvements require the development of either new materials with reduced parasitic absorption or new structures that break away from the traditional silicon heterojunction design. Examples of the former include wider bandgap silicon oxides and carbides [28]–[30], or indirect bandgap materials such as microcrystalline silicon. The difficulty, particularly for modified i-layers, is to maintain the two key functions

performed by a-Si:H—passivation and conduction—while increasing transparency or reducing recombination. We anticipate that OPAL models and test structures with omitted layers will be instrumental in evaluating these new materials, as the approach presented here can be used for new layers provided the optical constants are known. The most prominent example of the latter approach is the interdigitated back-contact architecture [31], for which maintaining passivation while electrically separating the emitter and back-surface field is an ongoing challenge.

ACKNOWLEDGMENT

We thank Y. Andrault for wafer preparation.

REFERENCES

[1] T. Mishima, M. Taguchi, H. Sakata, and E. Maruyama, "Development status of high-efficiency HIT solar cells," *Solar Energy Mater. Solar Cells*, vol. 95, pp. 18–21, Jan. 2011.

[2] S. Harrison, A. Danel, G. D'Alonzo, C. Arnal, P. E. Hickel, D. Munoz, and P. J. Ribeyron, "Towards industrialization of a-Si:H/c-Si heterojunction cells: From 20.5% record cells to 19.8% efficiency on industry compatible 148.5 cm^2 CZ wafers," presented at the 37th IEEE Photovoltaic Spec. Conf., Seattle, WA, Jun. 19–24, 2011.

[3] D. Psych, C. Meinhardt, K.-U. Ritzau, M. Bivour, K. Zimmermann, C. Schetter, M. Hermle, and S. W. Glunz, "Comparison of intrinsic amorphous silicon buffer layers for silicon heterojunction solar cells deposited with different PECVD techniques," presented at the 35th IEEE Photovoltaic Spec. Conf., Honolulu, HI, Jun. 20–25, 2010.

[4] A. Descoeudres, L. Barraud, R. Bartlome, G. Choong, S. De Wolf, F. Zicarelli, and C. Ballif, "The silane depletion fraction as an indicator for the amorphous/crystalline silicon interface passivation quality," *Appl. Phys. Lett.*, vol. 97, pp. 183505-1–183505-3, Nov. 2010.

[5] A. Descoeudres, L. Barraud, S. De Wolf, B. Strahm, D. Lachenal, C. Guerin, Z. C. Holman, F. Zicarelli, B. Demaurex, J. Seif, J. Holovsky, and C. Ballif, "Improved amorphous/crystalline silicon interface passivation by hydrogen plasma treatment," *Appl. Phys. Lett.*, vol. 99, pp. 123506-1–123506-3, Sep. 2011.

[6] J. I. Pankove and M. L. Tarng, "Amorphous silicon as a passivant for crystalline silicon," *Appl. Phys. Lett.*, vol. 34, pp. 156–157, Jan. 1979.

[7] H. Matsuura, T. Okuno, H. Okushi, and K. Tanaka, "Electrical properties of n-amorphous/p-crystalline silicon heterojunctions," *J. Appl. Phys.*, vol. 55, pp. 1012–1019, Feb. 1984.

[8] M. Taguchi, E. Maruyama, and M. Tanaka, "Temperature dependence of amorphous/crystalline silicon heterojunction solar cells," *Jpn. J. Appl. Phys.*, vol. 47, pp. 814–818, Feb. 2008.

[9] T. F. Schulze, L. Korte, E. Conrad, M. Schmidt, and B. Rech, "Electrical transport mechanisms in a-Si:H/c-Si heterojunction solar cells," *J. Appl. Phys.*, vol. 107, pp. 023711-1–023711-13, Jan. 2010.

[10] H. Fujiwara and M. Kondo, "Effects of a-Si:H layer thicknesses on the performance of a-Si:H/c-Si heterojunction solar cells," *J. Appl. Phys.*, vol. 101, pp. 054516-1–054516-9, Mar. 2007.

[11] M. Tanaka, M. Taguchi, T. Matsuyama, T. Sawada, S. Tsuda, S. Nakano, H. Hanafusa, and Y. Kuwano, "Development of new a-Si/c-Si heterojunction solar cells: ACJ-HIT (artificially constructed junction-heterojunction with intrinsic thin-layer)," *Jpn. J. Appl. Phys.*, vol. 31, pp. 3518–3522, Nov. 1992.

[12] N. Jensen, R. M. Hausner, R. B. Bergmann, J. H. Werner, and U. Rau, "Optimization and characterization of amorphous/crystalline silicon heterojunction solar cells," *Prog. Photovoltaics: Res. Appl.*, vol. 10, pp. 1–13, Jan. 2002.

[13] M. R. Page, E. Iwaniczko, Y.-Q. Xu, L. Roybal, F. Hasoon, Q. Wang, and R. S. Crandall, "Amorphous/crystalline silicon heterojunction solar cells with varying i-layer thickness," *Thin Solid Films*, vol. 519, pp. 4527–4530, May 2011.

[14] M. Buchanan, J. B. Webb, and D. F. Williams, "Preparation of conducting and transparent thin films of tin-doped indium oxide by magnetron sputtering," *Appl. Phys. Lett.*, vol. 37, pp. 213–215, Jul. 1980.

[15] H. Fujiwara and M. Kondo, "Effects of carrier concentration on the dielectric function of ZnO:Ga and In_2O_3:Sn studied by spectroscopic ellipsometry: Analysis of free-carrier and band-edge absorption," *Phys. Rev. B*, vol. 71, pp. 075109-1–075109-10, Feb. 2005.

[16] S. C. Baker-Finch and K. R. McIntosh, "Reflection of normally incident light from silicon solar cells with pyramidal texture," *Prog. Photovoltaics: Res. Appl.*, vol. 19, pp. 406–416, Jun. 2011.

[17] S. C. Baker-Finch and K. R. McIntosh, "A freeware program for precise optical analysis of the front surface of a solar cell," presented at the 35th IEEE Photovoltaic Spec. Conf., Honolulu, HI, Jun. 20–25, 2010.

[18] E. Burstein, "Anomalous optical absorption limit in InSb," *Phys. Rev.*, vol. 93, pp. 632–633, Feb. 1954.

[19] T. S. Moss, "The interpretation of the properties of indium antimonide," in *Proc. Phys. Soc. B*, vol. 67, pp. 775–782, Oct. 1954.

[20] I. Hamberg and C. G. Granqvist, "Evaporated Sn-doped In_2O_3 films: Basic optical properties and applications to energy-efficient windows," *J. Appl. Phys.*, vol. 60, pp. R123–R159, Dec. 1986.

[21] N. Jensen, U. Rau, R. M. Hausner, S. Uppal, L. Oberbeck, R. B. Bergmann, and J. H. Werner, "Recombination mechanisms in amorphous silicon/crystalline silicon heterojunction solar cells," *J. Appl. Phys.*, vol. 87, pp. 2639–2645, Mar. 2000.

[22] C. C. Tsai, G. B. Anderson, R. Thompson, and B. Wacker, "Control of silicon networks structure in plasma deposition," *J. Non-Cryst. Solids*, vol. 114, pp. 151–153, Dec. 1989.

[23] M. J. Powell and S. C. Deane, "Improved defect-pool model for charged defects in amorphous silicon," *Phys. Rev. B*, vol. 48, pp. 10815–10827, Oct. 1993.

[24] S. De Wolf and M. Kondo, "Nature of doped a-Si:H/c-Si interface recombination," *J. Appl. Phys.*, vol. 105, pp. 103707-1–103707-6, May 2009.

[25] T. F. Schulze, C. Leendertz, N. Mingirulli, L. Korte, and B. Rech, "Impact of Fermi-level dependent defect equilibration on V_{oc} of amorphous/crystalline silicon heterojunction solar cells," *Energy Procedia*, vol. 8, pp. 282–287, Apr. 2011.

[26] R. Stangl, M. Kriegel, and M. Schmidt, "AFORS-HET, version 2.2, A numerical computer program for simulation of heterojunction solar cells and measurements," presented at the 4th World Conf. Photovoltaic Energy Convers., Waikoloa, HI, May 8–12, 2006.

[27] S. De Wolf and G. Beaucarne, "Surface passivation properties of boron-doped plasma-enhanced chemical vapor deposited hydrogenated amorphous silicon films on p-type crystalline Si substrates," *Appl. Phys. Lett.*, vol. 88, pp. 022104-1–022104-3, Jan. 2006.

[28] H. Fujiwara, T. Kaneko, and M. Kondo, "Application of hydrogenated amorphous silicon oxide layers to c-Si heterojunction solar cells," *Appl. Phys. Lett.*, vol. 91, pp. 133508-1–133508-3, Sep. 2007.

[29] D. Pysch, M. Bivour, M. Hermle, and S. W. Glunz, "Amorphous silicon carbide heterojunction solar cells on p-type substrates," *Thin Solid Films*, vol. 519, pp. 2550–2554, Feb. 2011.

[30] T. Mueller, S. Schwertheim, M. Scherff, and W. R. Fahrner, "High quality passivation for heterojunction solar cells by hydrogenated amorphous silicon suboxide films," *Appl. Phys. Lett.*, vol. 92, pp. 033504-1–033504-3, Jan. 2008.

[31] N. Mingirulli, J. Haschke, R. Gogolin, R. Ferré, T. F. Schulze, J. Düsterhöft, N.-P. Harder, L. Korte, R. Brendel, and B. Rech, "Efficient interdigitated back-contacted silicon heterojunction solar cells," *Phys. Status Solidi—Rapid Res. Lett.*, vol. 5, pp. 159–161, Apr. 2011.

Zachary C. Holman was born in Santa Cruz, CA, in 1984. He received the B.A. degree in physics from Reed College, Portland, OR, and the Ph.D. degree in mechanical engineering from the University of Minnesota, Minneapolis, MN, in 2005 and 2010, respectively.

In 2010, he joined the Photovoltaics and Thin-Film Electronics Laboratory, Ecole Polytechnique Fédérale de Lausanne, Neuchâtel, Switzerland, as a Postdoctoral Researcher. His research interests include light management in solar cells, high-efficiency silicon solar cells, and novel photovoltaic devices incorporating nanoparticles.

Antoine Descoeudres was born in Lausanne, Switzerland, in 1978. He received the M.Sc. and Ph.D. degrees in physics from Ecole Polytechnique Fédérale de Lausanne, Lausanne, Switzerland, in 2001 and 2006, respectively.

From 2007 to 2009, he was a Postdoctoral Researcher at the European Laboratory for Particle Physics, Geneva, Switzerland, studying vacuum breakdowns for the development of high-gradient accelerating cavities. Since 2009, he has been a Researcher at the Photovoltaics and Thin-Film Electronics Laboratory, Ecole Polytechnique Fédérale de Lausanne in Neuchâtel, Switzerland. His current research interests include thin-film deposition with plasma-enhanced chemical vapor deposition and plasma diagnostics for the development of silicon heterojunction solar cells.

Loris Barraud was born in Le Locle, Switzerland, in 1985. He received the Diplôme Ingénieur HES degree in microtechnology from the Ecole d'ingénieur du Locle in 2009.

In 2009, he joined the Photovoltaics and Thin-Film Electronics Laboratory, Ecole Polytechnique Fédérale de Lausanne, Neuchâtel, Switzerland, as a Scientific Collaborator. His research interests include thin-film deposition for solar cells.

Fernando Zicarelli Fernandez was born in Michigan in 1964.

He is a Degreed Engineer and has been in the industrial microelectronics and photovoltaics sector for 20 years. In 2009, he joined the Photovoltaics and Thin-Film Electronics Laboratory, Ecole Polytechnique Fédérale de Lausanne, Neuchâtel, Switzerland, as a Metallization Expert. His research interests include reduction of silver paste linewidths in solar cells using screen printing technology.

Johannes P. Seif was born in Tübingen, Germany, in 1984. After starting physics studies at the University of Tübingen in 2004, he went to the Swiss Federal Institute of Technology, Zürich, Switzerland, in 2006, where he received the Master's degree in physics in 2009.

He did a six-month Internship at Oerlikon Solar, Trübbach, Switzerland. He joined the Photovoltaics and Thin-Film Electronics Laboratory, Ecole Polytechnique Fédérale de Lausanne, Neuchâtel, Switzerland, for a Ph.D. thesis in 2010. His research interests include high-efficiency solar cells, as well as transport and optical properties of thin amorphous and microcrystalline layers.

Stefaan De Wolf received the Ph.D. degree from the Catholic University of Leuven, Leuven, Belgium, while he was with Interuniversity Microelectronics, Leuven, focusing on crystalline silicon solar cells.

From 2005 to 2008, he was with the National Institute of Advanced Industrial Science and Technology, Tsukuba, Japan, focusing on silicon heterojunction devices. In 2008, he joined the Photovoltaics and Thin-Film Electronics Laboratory, Ecole Polytechnique Fédérale de Lausanne, Neuchâtel, Switzerland, as a Team Leader for activities on such solar cells.

Christophe Ballif received the Graduate's degree in physics and Ph.D. degree from Ecole Polytechnique Fédérale de Lausanne (EPFL), Lausanne, Switzerland, in 1994 and 1998, respectively, focusing on novel photovoltaic materials.

He was a Postdoctoral Researcher at National Renewable Energy Laboratory, Golden, CO, where he was involved in compound semiconductor solar cells (CIGS and CdTe). He then was with the Fraunhofer Institute for Solar Energy Systems, Freiburg, Germany, where he was involved in crystalline silicon photovoltaics (monocrystalline and multicrystalline) until 2003. He then joined the Swiss Federal Laboratories for Materials Testing and Research, Thun, Switzerland, before becoming a Full Professor and Chair at the Institute of Microengineering, University of Neuchâtel, Neuchâtel, Switzerland, in 2004. In 2009, the Institute of Microengineering was transferred to Ecole Polytechnique Fédérale de Lausanne. He is the Director of the Photovoltaics and Thin-Film Electronics Laboratory within the Institute. His research interests include thin-film silicon, high-efficiency heterojunction crystalline cells, and module technology, contributing to technology transfer and industrialization of novel devices.